

CFD ANALYSIS OF THE BEHAVIOR OF AIRBORNE ALLERGENS IN CARPETED AND UNCARPETED DWELLINGS

Bradley A. Ciccirelli¹, David L. Davidson², Edward H. Hart and P. Robert Peoples
Solutia Inc.
3000 Old Chemstrand Rd.
Cantonment FL 32533

ABSTRACT

There is considerable concern today over indoor air quality (IAQ). The factors that influence IAQ may be numerous, and there is considerable research aimed at quantifying these factors. This research is of particular interest to industries that manufacture products used in residential and commercial dwellings, such as the carpet industry. With respect to carpet, there are various opinions about its role in IAQ, but little quantitative data. Much of the quantitative data that does exist either ignores or makes crude assumptions about the influence of fluid dynamics on the experimental observations.

In this paper we discuss our use of Computational Fluid Dynamics (CFD) to model the transient behavior of airborne particles in dwellings with and without carpeted floors to quantify the impact of floor covering on IAQ. In particular, we discuss the theoretical considerations that are required to construct an accurate and practical CFD model that captures the correct fluid and particle dynamics, and present and summarize CFD predictions that account for the effects of HVAC systems, room geometry and virtual objects, such as people moving about the dwelling.

In addition to getting the fluid and particle dynamics correct, there are two additional aspects of this problem that will be discussed. First, in order to draw reasonable conclusions about IAQ, a large number of simulations are required to capture the wide range of realistic dwelling conditions of interest. In order to perform these simulations in a timely manner, the process of building and meshing the geometry, specifying all relevant room conditions, conducting the simulation and interrogating the results has been automated by constructing a *Digital Expert* for the problem, wherein the user can automatically complete these tasks with little CFD expertise and no intervention.

Second, it is essential to communicate the results of these simulations to lay audiences – the wide range of people interested in IAQ, including school boards, politicians and other government officials. We have developed a means of generating “Hollywood grade” animations that are more realistic in appearance than conventional CFD animations, and consequently more appealing and more readily understandable, but that reflect the correct fluid and particle dynamics. We believe that the integration of CFD with realistic animation capability will see greater applicability as our society becomes increasingly dependent on technology and decreasingly technically literate.

INTRODUCTION

Over the last 25 years, substantial effort has been focused on the study of indoor air contaminants, starting with chemical exposures and eventually including airborne particles. Interest in the latter is the result of 1) research that associates small particles with increased mortality (Creason, et al., 2001), and 2) observations of a dramatic increase in reported asthma in the last 30 years (Lang and Sears, 2001), which correlates with the evidence that most Americans presently spend about 90% of their time indoors. The economic impact of asthma and allergy is significant as well. The direct cost of asthma morbidity and mortality in 1998 in the United States alone was estimated at \$12.7 billion (Weiss and Sullivan, 2002).

The etiology of asthma is apparently intricate, but many of the triggers are believed to be airborne allergens. While considerable attention has been given to experimental measurement of airborne allergens in dwellings, little attention has been given to the fluid and particle mechanics that dictate particle motion. Consequently, the development of an understanding of the exposures and associated risks has been difficult to obtain. Factors such as settling rates, multiple primary sources, re-suspension rates, effects of turbulence, and affinities for interior surfaces make it a challenge to accurately quantify exposures.

In this paper we discuss the application of computational fluid dynamics to the airborne allergen problem, to show that it is the appropriate tool and to generate some initial results regarding the relative impact of carpeted and uncarpeted floors on airborne allergen concentration.

PROBLEM DEFINITION

The domains of interest are residential, commercial, governmental and other types of dwellings. As such, the geometry must account for rooms of various sizes, interior walls and passageways, HVAC systems and floor coverings. A typical domain is illustrated in Figure 1, a four room residence with an HVAC inlet in the ceiling of each room, one HVAC return in an exterior wall of one room, two carpeted surfaces

and two uncarpeted surfaces. In principle, the dwelling can be as simple as a single room or as complicated as desired.

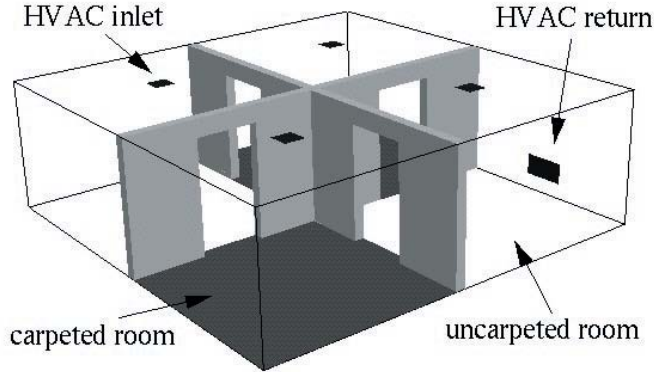


Figure 1. Geometry of four room dwelling showing carpeted and uncarpeted surfaces, walls and interior passageways, HVAC inlets and returns.

Flow in the dwelling can be induced by the HVAC system and by moving occupants. Buoyant and other thermal effects are not considered in the present work³, **hence the air flow is essentially incompressible. The airborne allergen particles of interest are typically between 2 and 40 μm in average diameter**, and have densities on the order of $1\text{-}3 \times 10^3 \text{ kg/m}^3$.

The problem is inherently transient, in view of typical HVAC cycles and traffic patterns in typical dwellings of all types, and of course three dimensional. A simulation can be started at any stage, of course, but certain scenarios are convenient. For example, it is convenient to uniformly seed the dwelling at a particular particle concentration and then devote the first portion of the simulation to particle settling (HVAC off), prior to cycling the HVAC or introducing a moving occupant. Furthermore, particles can enter and leave the domain through the HVAC inlets and returns, and the inlet particle concentration can be set at will, to correspond to perfectly filtered air (inlet particle concentration = zero) or unfiltered air (inlet particle concentration specified). Presently the inlets and returns of the HVAC system are not connected, which provides an additional degree of freedom.

CFD MODEL

Particle Model

In general, a fluid-borne particle dynamics problem is a multiphase flow problem. However, the regime of interest allows us to make certain simplifications that reduce the complexity of the simulation without sacrificing accuracy.

First, the response times of the particles of interest are much smaller than the characteristic convection time scales in the dwelling. A force balance on a single spherical particle that obeys Stokes drag reveals that the response time, that is the time required for the particle to accelerate to the local fluid velocity, is

$$t_p = \frac{\rho_p R_p^2}{9\eta} \quad (1)$$

where ρ_p , R_p and η represent the solid particle density, particle radius and air viscosity, respectively. For a spherical $40 \mu\text{m}$ diameter particle of 3000 kg/m^3 density in air at room temperature, $t_p = 7.4 \text{ ms}$. This is at least two orders of magnitude smaller than typical convection time scales. Thus, we assume that particle acceleration is unimportant, so that the particles move according to the sum of the local fluid velocity and the particle settling (slip) velocity everywhere within the dwelling at all times.

Second, the particle concentrations of interest are very dilute, typically less than 10^{-4} volume fraction. Thus, the particle motion does not have a significant impact on the flow field or on the motion of other particles. The combination of these two factors permits the problem to be treated as a single phase flow problem, where the particle phase is continuous and behaves like a passive scalar, with the addition of a vertical velocity component equal to the particle settling velocity. This is the so-called algebraic slip model⁴, **which is described in greater detail elsewhere (AEA Technology, CFX4.4, Volume 3, 2001).**

Carpet Model

Carpet is geometrically quite complicated, and this complexity must be accounted for by some sort of spatial averaging. Figure 2 shows an electron micrograph of the tip of a typical carpet tuft. The scale indicates that the individual filament diameter⁵ **is on the order of $60 \mu\text{m}$** , and that the spaces between filaments are somewhat larger. In fact, carpets are mostly air, with void fractions on the order of 0.9. Clearly, there is sufficient space in typical carpet tufts for allergen particles to fall into the carpet tufts and, under certain conditions, to remain there.

The obvious approach is to model the carpet as a porous medium that obeys Darcy's law,

$$\underline{v} = -\underline{R}^{-1} \cdot \nabla p \quad (2)$$

where \underline{v} represents the local fluid velocity, p the local fluid pressure and \underline{R} the resistance tensor for the porous medium. This is a physically appropriate means of representing the detailed fibrous structure of a carpet, providing that the physical properties of the porous medium, the void fraction and permeability (or resistance) tensor, are obtained from a sensible physical analysis of the fibrous structure/fluid interaction or from a valid experiment. Void fraction is readily obtained from the details of carpet construction⁶. The resistance tensor can be *estimated* from drag correlations for fibrous porous media (Dullien, 1992), or from a more fundamental consideration, such as by treating the carpet as a regular array of cylinders and applying known or computed drag relationships.

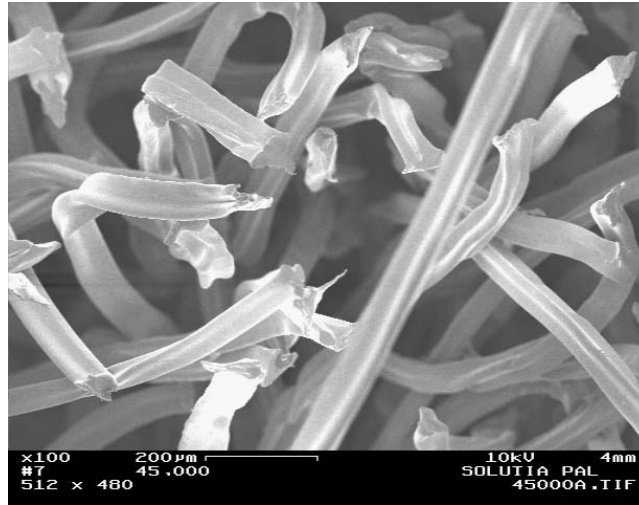


Figure 2. Electron micrograph showing structure of a typical carpet tuft (after service), illustrating approximate size of void regions.

In the latter case, it is easy to show that the resistance to flow normal to the axes of the cylinders is given by

$$R_{\perp} = \frac{\eta \text{Re}}{4r} C_D(\text{Re}) \langle \frac{A}{V} \rangle \quad (3)$$

where R_{\perp} represents the magnitude of the resistance tensor, r the filament radius, Re the filament Reynolds number ($2\rho U r/\eta$), C_D the drag coefficient, $\langle A/V \rangle$ the filament surface area per unit of occupied volume, ρ the air density and U the free stream air speed. The drag coefficient over a wide range of Reynolds numbers has been measured experimentally (Perry, 1997) and has been computed analytically at lower Reynolds numbers. The expression (Batchelor, 1977)

$$C_D = \frac{8\pi}{\text{Re} \ln(7.4/\text{Re})} \quad (4)$$

agrees very well with the experimentally obtained curve found in Perry for $\text{Re} < 1$. For a 60 μm diameter circular fiber in room temperature air, this corresponds to $U < 0.25$ m/s. We do not expect air speed within the carpet to exceed this value, so this expression for the drag coefficient is appropriate. It turns out that the product $\text{Re} C_D$, which appears in the expression for the resistance, changes by only a factor of 3.3 as Re changes by two orders of magnitude, from 1.0 to 0.01, hence this expression for the resistance is not only physically sensible but it is relatively insensitive to local variation in the air velocity field. It also leads to predictions for the resistance comparable to known correlations for fibrous porous media, such as that given by Davies (Dullien, 1992). One advantage of the fundamental approach to estimating the resistance tensor is that it is possible to attempt to take into account the impact of non-round cross section, finite filament separation and filament orientation.

Typical carpet fiber cross sections are shown in Figure 3. These trilobal fibers clearly have higher $\langle A/V \rangle$ than round fibers. It is a straightforward task to digitize these images, compute perimeters and areas and correlate with convenient measures of trilobal filament geometry used in the trade, such as modification ratio⁷ (MR). From a sample of about 200 Solutia trilobal filaments we find that the area enhancement factor correlates extremely well with MR, according to

$$\frac{\langle A/V \rangle_{\text{trilobal}}}{\langle A/V \rangle_{\text{round}}} = 1 + 0.2488(\text{MR} - 1) \quad (5)$$

Typical carpet fibers exhibit MRs between one and four, hence the area enhancement factor can be as high as about 1.75.

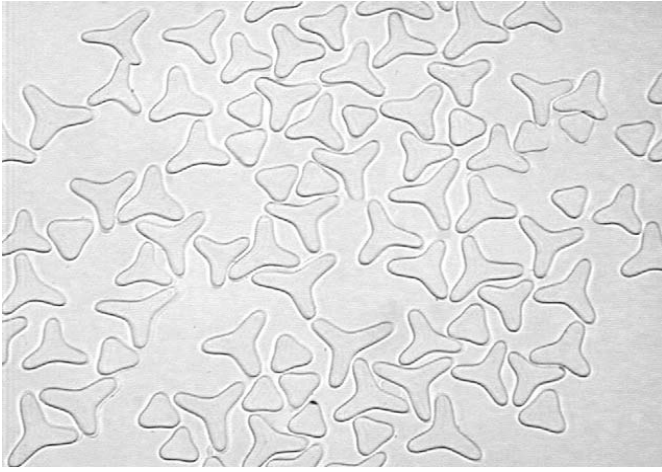


Figure 3. Visible micrograph showing typical carpet fiber cross sections illustrating high and low MR filaments.

The impact of cross section on drag can be estimated by applying CFD to real filament cross sections, such as those shown in Figure 3. Since the cross sections are irregular, we used an unstructured grid code to solve the problem (AEA Technology, *CFX-5*, 2001)^{8,9}. A typical grid in the vicinity of a trilobal filament is illustrated in Figure 4. The drag problem was defined in a three dimensional domain with symmetry planes defined on upper and lower planes and on the planes normal to the filament axis. The domain was a rectangular solid of prescribed size, with inlet 10 hydraulic diameters upstream of the filament axis, outlet 10 hydraulic diameters downstream of the filament axis, and upper and lower symmetry planes separated by a prescribed amount. We have found that 40 hydraulic diameters is equivalent to infinite separation for right circular cylinders. The inlet velocity was prescribed to be uniform over the inlet, and the mass flow at the outlet was specified accordingly. The results don't change significantly if the outlet pressure is applied instead for $Re \leq 1$.

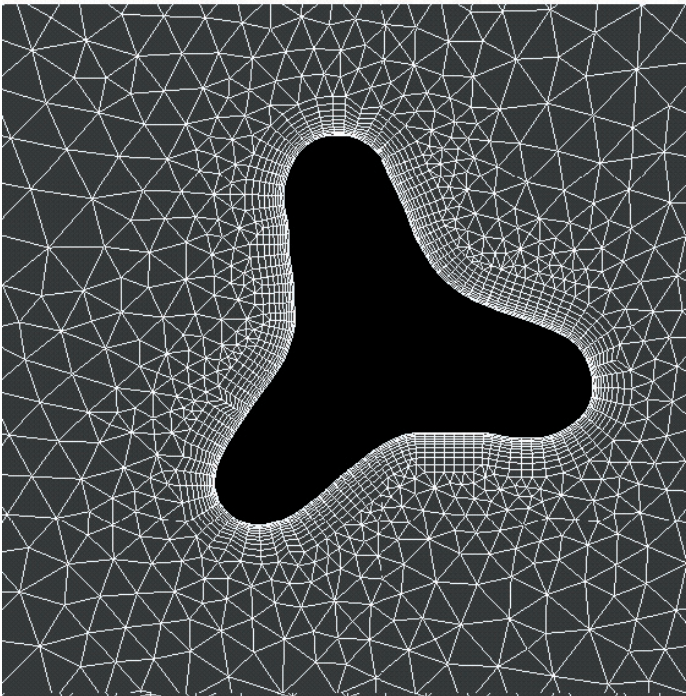


Figure 4. Typical mesh in the vicinity of a filament.

As indicated by Figure 5, these calculations reveal that the drag coefficient enhancement due to cross section shape¹⁰ is nearly independent of MR for $1.9 < MR < 2.9$ and filament Reynolds number¹¹ for $0.01 < Re < 1.0$, and is approximately equal to 1.3. The drag coefficient is defined in terms of hydraulic diameter¹², not filament extent normal to the flow. Presumably the drag enhancement is 1.3 at lower Reynolds numbers as well.

While drag enhancement due to cross section shape is modest, it depends strongly on average filament separation distance. Average filament separation distance can be computed from the details of carpet construction, and it turns out to be 2-4 filament diameters for typical constructions, consistent with the micrograph of Figure 2. The computational results shown in Figure 6 indicate that, in this range, drag coefficient enhancement is on the order of 2.5-10.5.

Drag Enhancement

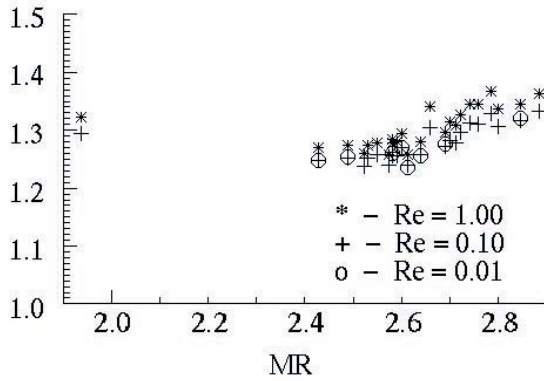


Figure 5. Enhancement of drag coefficient by trilobal cross section as a function of MR and Reynolds number.

Drag Enhancement

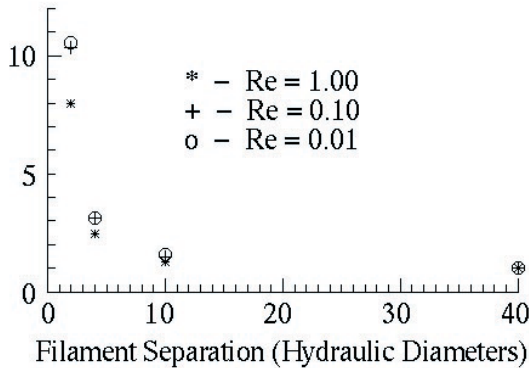


Figure 6. Enhancement of drag coefficient by circular cross section as a function of separation distance and Reynolds number.

When all of these factors are combined, we find that while the Davies correlation predicts the magnitude of the resistance tensor to be approximately $1-2 \times 10^4 \text{ kg/m}^3\text{-s}$, our array-of-filaments model predicts values about 20 times larger. Of course, the actual geometry of carpet tufts is more complicated in that fibers are not typically parallel over long distances, as indicated by Figure 2, which probably leads to even larger resistance and certainly less anisotropy. Thus, at the moment we can only state that the appropriate value for the resistance tensor is probably between 10^4 and $10^6 \text{ kg/m}^3\text{-s}$. Results reported herein treat the carpet as isotropic with a resistance tensor magnitude of $10^5 \text{ kg/m}^3\text{-s}$ and void fraction of 0.9.

Traffic Model

Pedestrian traffic is simulated by imposing a velocity field in the domain according to the location and local motion of a virtual human being. A canonical motion is defined using Shout3D¹³ and Java script, the result being a set of data files that contain three dimensional position and velocity information for the virtual human walking in place, each data file corresponding to a particular time in the treadmill-like walking cycle. The digital resolution of the human is selected to provide a reasonable approximation of the human without undue computational burden. We typically use about 4000 spatial positions (each with a three dimensional velocity vector) to specify the human at all times, and 12 temporal positions to specify one walking cycle. The path of the virtual human and speed along the path in the dwelling is defined, and the treadmill motion is mapped onto this contour beginning at the specified time and subsequently throughout the CFD simulation of the dwelling. Linear interpolation between the 12 temporal positions is used to obtain the spatial positions and velocity vectors at the simulation times, since in general the integration step size used in the CFD simulation of the dwelling is not equal to the temporal interval used to define the virtual human motion.

The local velocity field is set equal to the human velocity field in every computational cell¹⁴ in which the human exists, and it is imposed on the solution at the appropriate locations using CFX-4 user FORTRAN subroutine USRSRC, as described elsewhere (AEA Technology, CFX4.4, Volume 2, 2001). In essence, at each node on which we impose virtual human motion, we overwrite the diagonal element of the coefficient matrix and the corresponding element of the constant vector of the linearized system of algebraic equations that results from discretization of the appropriate momentum conservation law, such that the solution at that node reduces to the imposed velocity component. This approach correctly captures the velocity field on the surface of the virtual human without requiring either unstructured or adaptive meshes. The excluded volume of the human is not taken into account. We believe that this omission does not have a significant impact on the results.

Contact Force Model

Presently our model ignores electrostatic and van der Waals interactions between carpet fibers and allergen particles, and we believe this is a conservative approach (Hedge, 2001). However, one can estimate the impact of particle-fiber attraction by estimating the particle-fiber collision probability within the carpet and subsequently removing particles that have collided with carpet fibers from the problem domain. In this respect, the carpet will behave like a fibrous filter wherein some fraction of the airborne particles that pass through the filter are irreversibly captured and retained by the filter. An elementary approach to this problem suggests that the collision rate $N_p [=] \text{volume of particles per volume of domain per second}^{15}$, should be approximately given by

$$N_p = \frac{V_p \epsilon D_p}{D_{sep}^2} \quad (6)$$

where V_p represents local particle speed, ϵ particle volume fraction, D_p particle diameter and D_{sep} the average filament separation distance. Results are presented in this paper with and without irreversible particle capture.

MODEL PREDICTIONS

The following results correspond to the single room dwelling with single HVAC inlet and single return shown in Figure 7. The room is 3.66 m X 3.66 m X 2.44 m with HVAC inlet centered 0.92 m from the corner in both directions. The return is centered 0.92 m from the nearest adjacent wall and 0.49 m from the floor. The HVAC circulation rate, when on, is 0.0564 m³/s. When the virtual human is in the domain, it corresponds approximately to an adult male walking in a 1.83 m circle centered at the center of the floor translating along the circle at 1.22 m/s. The computational grid is 40X40X40¹⁶, uniform in the plane parallel to the floor, uniform vertically in the first half inch (where the carpet resides) and progressively scaled upward from there. Note that the same grid is used with and without carpet. Simulation parameters are summarized in the Appendix.

In Figure 7, the virtual human is visualized by defining a user scalar (*human*) that is identically 1 in grid cells that contain the human and identically zero everywhere else. The image corresponds to an isosurface of *human*=0.5. It is shaded according to local speed. Note the higher speed of the left hand and the right foot in this particular image, which reflects normal walking.

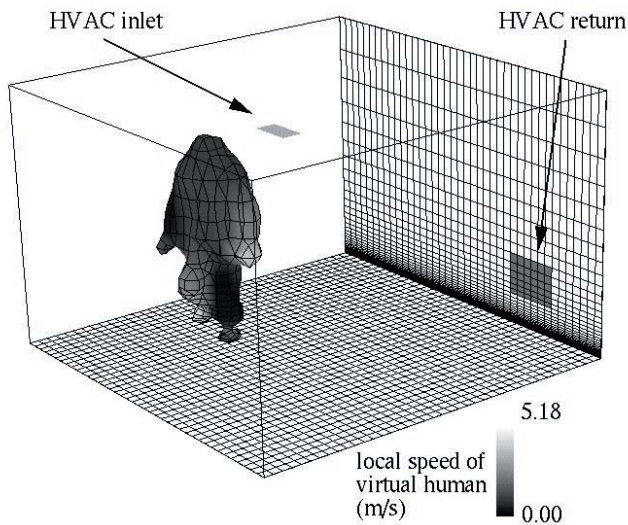


Figure 7. Single room showing HVAC inlet in ceiling, HVAC return, uniform mesh parallel to floor, non-uniform vertical mesh and virtual human.

Figure 8 compares the concentration of 5 μm airborne particles, spatially averaged over the cross section of the room, at approximately child height and adult height over 8-9 HVAC cycles, each cycle consisting of ten minutes off followed by one minute on. In both cases, the room was initially uniformly filled with particles at 10⁻⁴ volume fraction. The upper set of curves correspond to unfiltered HVAC inlet air with particle loading of 10⁻⁴ volume fraction, and the lower to perfectly filtered inlet air. Irreversible particle capture by the carpet does not occur.

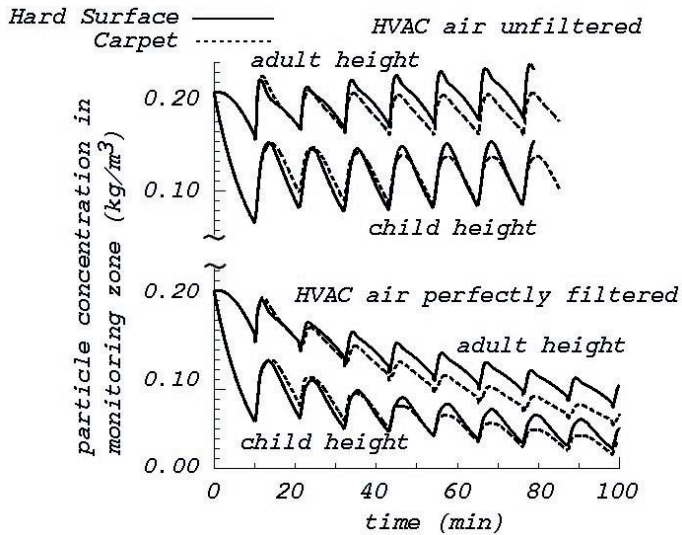


Figure 8. Instantaneous time dependent concentration of 5 μm diameter particles in adult and child breathing zones over multiple HVAC cycles without particle capture; hard vs. carpeted surface; 40X40X20 grid.

The drop in concentration in every cycle when the HVAC system is off is due to particle settling, of course. The settling velocity of an isolated spherical particle under the influence of Stokes drag for $\text{Re} < 0.1$ is given by

$$v_s = \frac{2R_p^2 \rho_p g}{9\eta} \quad (7)$$

where v_s represents particle settling velocity and g acceleration due to gravity. For the particles used in this simulation, the settling velocity is 0.00148 m/s and at that velocity the particle Reynolds number is 4.8×10^{-4} . As the particles settle to the floor, if the floor is carpeted, they enter the carpet and remain there until they are swept out by the air currents caused by the HVAC system. However, the carpet offers a greater resistance to air flow than the corresponding volume of unfilled space at the floor in the uncarpeted case, hence the particles are more difficult to dislodge. This leads to lower concentrations in the breathing zones over time. In this particular case, the HVAC flow, when on, was 0.0564 m^3/s , which corresponds to an average residence time for the room of 578 s = 9.6 min. For a perfectly mixed room with this residence time, the concentration would drop from 0.2 to 0.0736 kg/m^3 in one residence time, which is fairly close to the average concentration in the room after nine HVAC cycles¹⁷.

Figure 9 illustrates spatially averaged concentration in the adult breathing zone for the same room during a 40 second walk by the virtual human after 10 minutes of quiescent settling. The room was initially uniformly filled with 2, 5 and 10 μm diameter particles, each at 10^{-4} volume fraction. The HVAC system was off throughout the simulation. The settling velocity of the 10 μm particle is 0.592 m/s, which corresponds to a particle Reynolds number of 3.82×10^{-3} .

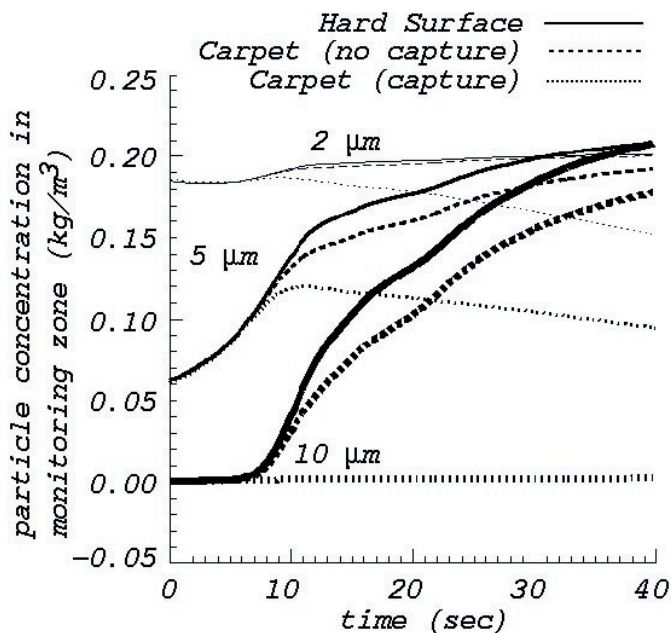


Figure 9. Instantaneous time dependent concentration of 2, 5 and 10 μm diameter particles in adult breathing zone during 40 second walk period, after 10 minute settling period; hard vs. carpeted surfaces, with and without particle capture; 40X40X40 grid.

At the beginning of the walking period, the 10 μm particles have completely settled below the adult breathing zone, whereas the 5 μm particles have not, although the concentration of the latter is about $\frac{1}{4}$ of the initial concentration at that point. The 2 μm particles have settled very little. The velocity field is entirely induced by the motion of the virtual human, who circles the center of the room as described previously. The combined action of his translation and local motion, particularly the feet moving near the floor, stirs up the particles substantially, as indicated by the figure. Again, there is a clear difference between carpet (without capture) and hard surface, due to the greater resistance to flow offered by the carpet, which makes it more difficult to dislodge particles. The impact of irreversible particle entrapment, based on collision probability, leads to a further and substantial decrease in airborne particle concentration.

The impact of irreversible particle entrapment is also shown in Figure 10 for 2, 5, 10 and 20 μm particles. The conditions of this simulation are otherwise identical to those that correspond to Figure 8. The difference is striking but not completely surprising. In this case the carpet behaves much like a fibrous filter, retaining airborne particulates until they can be removed by vacuuming, whereas a hard surface cannot retain the particles and they remain airborne at much higher concentrations.

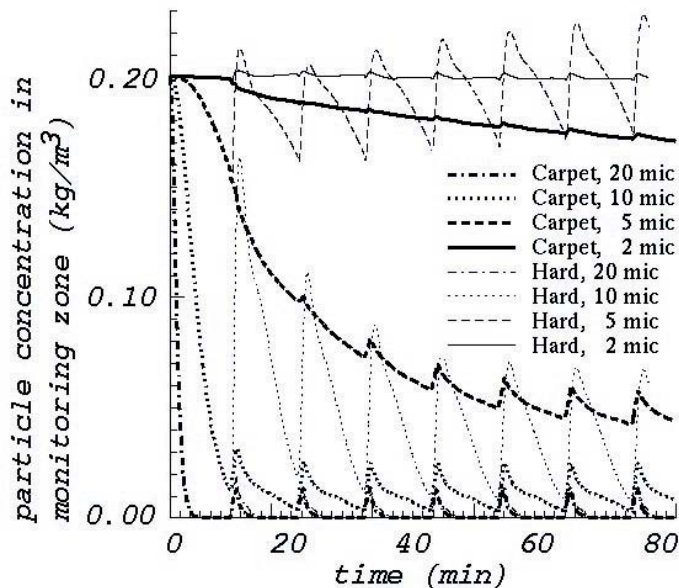


Figure 10. Instantaneous time dependent concentration of 2, 5, 10 and 20 μm diameter particles in child breathing zone over multiple HVAC cycles with irreversible particle capture; hard vs. carpeted surface; 40X40X20 grid.

DIGITAL EXPERT

The results presented in this paper provide clear indications about the impact of carpeted flooring on airborne particle concentrations, and that CFD is the appropriate tool to study the issue. One can easily imagine a large number of scenarios worth investigating, such as various room configurations, HVAC systems and cycles, traffic patterns and particle characteristics. Thus, we expect to use this model frequently.

In order to facilitate use, we have constructed a *Digital Expert* for the problem (Davidson, 2001), a tailor-made CFD tool that allows the user to solve meaningful engineering problems around some area of technology or some manufacturing operation without any knowledge of CFD or CFD packages whatsoever. Digital experts have an important place in industry today, in both off-line and on-line applications. There is in fact one commercial example of a tool designed to facilitate the construction of digital experts by in-house experts (Dewhurst, 2001).

Presently, one need only fill out a table that completely defines the problem, specify the number of CPUs to run the simulation on and submit it. The geometry is built and meshed from scratch and all physical and simulation control information written to the appropriate CFX-4 command file. User FORTRAN is used extensively to control and monitor the simulation as well. The digital expert maintains an archive of cases with both input and output information to permit organization of the results.

Post processing is accomplished with user FORTRAN and FIELDVIEW 8.0 (Intelligent Light, 2001)¹⁸.

HOLLYWOOD ANIMATION

The intended audience for the ultimate results and conclusions of this work is primarily non-technical, for which the format typically used for scientific results is not optimal. To this end, we have developed a method of rigorously transforming the CFD results into what we call *Hollywood-grade* animations that preserve the quantitative aspects of the results but cast them into a more readily understandable format.

Our approach uses a combination of FIELDVIEW, 3D Studio Max¹⁹ and Perl, which allows us to convert images such as that shown in Figure 7 into images such as those shown in Figure 11. The spatially and temporally dependent field variables are extracted from the

CFD results file with FIELDVIEW, and converted to particles and particle motions with 3D Studio Max and Perl. When such animations are incorporated into self-contained presentations that provide the appropriate auxiliary information, such as quantitative comparisons and specification of conditions, we believe they are much more effective with non-technical audiences.

SUMMARY

Although indoor air quality has been a popular research topic for the last 25 years or so, little or no attention has been given to the importance of fluid and particle mechanics to the issue. In fact, a complete understanding of the relevant fluid and particle mechanics is essential not only to a complete understanding of indoor air issues, but also to appropriate design and interpretation of IAQ experiments. It is common practice to put particle and chemical samplers in rooms, record measurements and draw conclusions with no regard for or discussion of the fluid and particle mechanics.

In this paper we have shown that computational fluid dynamics is ideally suited for the careful study of IAQ issues, and that the complications associated with dwelling geometry, particle dynamics, porous media such as carpet, traffic patterns and HVAC cycles can be dealt with in a reasonable fashion.

CFD simulations on a model single room with and without carpet indicate that there is a significant impact of floor covering on airborne particle concentration, which is lower if the floor is carpeted as opposed to a hard surface. This difference can be great if the carpet irreversibly traps particles that collide with the carpet fibers, due to the much greater surface area available for particle collision in a fibrous carpet compared to that of a hard surface. The impact of carpet on allergic responses can be great both in terms of instantaneous and long term exposure.

To facilitate repetitive simulation of various scenarios, we have embedded the CFD simulation within a digital expert. Furthermore, we have combined a variety of commercially available CFD, visualization and rendering tools with our own code to convert the quantitative results provided by CFD to Hollywood-grade animations that are faithful to the CFD predictions but that are visually more appealing to the non-technical audience that this work is primarily intended for. We believe that both digital experts and Hollywood-grade rendering of CFD results will become increasingly important as the use of technology continues to outstrip technical literacy.

Figure 11. Several frames from Hollywood-grade animation. Frame sequence is top to bottom.

ACKNOWLEDGMENTS

We wish to acknowledge Lori Ables and Grady Hill of Solutia for providing the electron and visible micrographs, Alan Luedtke of DuPont for helpful discussions, and the Carpet and Rug Institute for assisting and supporting this work.

NOMENCLATURE

A filament surface area (m^2)
 C_D drag coefficient



D_p

particle diameter (m)

D_{sep}	average filament separation distance in carpet (m)
MR	modification ratio for trilobal filament
N_p	particle-filament collision rate (s^{-1})
R_{\perp}	magnitude of resistance tensor ($kg/m^3 \cdot s$)
\underline{R}	resistance tensor for porous medium ($kg/m^3 \cdot s$)
R_p	particle radius (m)
Re	Reynolds number
U	free stream air speed (m/s)
V	volume occupied by a filament in carpet (m^3)
V_p	local particle speed (m/s)
g	gravitational acceleration (m/s^2)
p	local fluid pressure ($kg/m \cdot s^2$)
r	filament radius (m)
t_p	particle response time (s)
\underline{v}	local fluid velocity vector (m/s)

v_s particle settling velocity (speed) (m/s)

Greek

ϵ particle volume fraction

η air viscosity (kg/m-s)

ρ_p solid particle density (kg/m³)

Symbols

<> denotes average over all filaments in a carpet

Subscripts

o denotes circular cross section

∴ denotes trilobal cross section

REFERENCES

AEA Technology Engineering Software, *CFX-4.4: Solver*, Volume 2, pp3-567 – 3-571, 2001.

AEA Technology Engineering Software, *CFX-4.4: Solver*, Volume 3, p3-793, 2001.

AEA Technology Engineering Software, *CFX-4.4: Solver*, Volume 3, p3-793, 2001.

Batchelor, G. K., *An Introduction to Fluid Dynamics*, Cambridge, London, section 4.10, 1977.

Creason, J., Neas, L., Walsh, D., Williams, R., Sheldon, L., and Shy, C., *J. Exposure Analysis and Epidemiology*, **11**, 1-7, 2001.

Davidson, D. L., “SpinExpert – The Digital Expert for the Analysis and Design of Fiber Spinning Operations,” *Proceedings of 3rd International ASME Symposium on Computational Technology (CFD) for Fluid/Thermal/Chemical/Stress Systems and Industrial Applications*, Atlanta, 2001.

Dewhurst, S., “Enterprise Accessible Software Applications,” *CFXUpdate*, No. 21, Winter 2001.

Dullien, F. A. L., *Porous Media Fluid Transport and Pore Structure*, Academic Press, San Diego, section 3.2.3, 1992.

Hedge, A., *Human Ecology*, Cornell University Press, Spring 2001.

Intelligent Light, *FIELDVIEW User's Guide*, version 8.0, 2001.

Perry, R.H. and Green, D.W., editors, *Perry's Chemical Engineers' Handbook*, 7th Edition, McGraw Hill, p6-51, 1997.

Platts-Mills, T. A. E. et al, *Bulletin of the World Health Organization*, **66**, 769-780, 1988.

Lang, David M. and Sears, M. R., *Annals of Allergy, Asthma, & Immunology*, **87**, 91, 2001.

Weiss, K. B. and Sullivan, S. D., *Journal of Allergy & Clinical Immunology*, **107**, 38, 2002.

⁷ Modification ratio is defined as the ratio of diameters of the circumscribed and inscribed circles that can be constructed on each cross section. Thus $MR=1$ corresponds to a perfect circle.

⁸ www.software.aeat.com/cfx.

⁹ This is an example of the advantage of using commercial CFD codes outside of the gui. The sheer number of distinct cross sections and their orientations (they are not symmetric about their axes) can lead to thousands of individual simulations required to construct a complete drag curve. Using a little FORTRAN and a template CFX-5 session file (and lots of CPU cycles) we can completely automate the process of generating the simulated drag curves.

¹⁰ Defined as the ratio of drag coefficient of a particular cross section to drag coefficient of a circular cross section of equal hydraulic diameter.

¹¹ It is our intention to thoroughly study these drag relationships over a larger set of filament cross sections, but these results represent the extent of our computations at the time of this writing.

¹² Hydraulic diameter is used since it is independent of filament orientation.

¹³ www.shout3d.com.

¹⁴ The grid used to define the virtual human and the computational (CFD) grid imposed on the dwelling are independent, although the final resolution of the virtual human in the CFD simulation does depend on both grids. In most cases, we set the human grid resolution much higher than the dwelling grid resolution, whereby in a particular dwelling grid cell, the nodal velocity is set to the average velocity of all virtual human nodes that are within that grid cell at that particular time.

¹⁵ This rate is needed in terms of particle volume since we are using the algebraic slip model and solving for the field variable of particle volume fraction.

¹⁶ 40X40X20 was used as well in some simulations.

¹⁷ This is offered merely as a rough check on the CFD calculations.

¹⁸ www.ilight.com.

¹⁹ www.discreet.com.